

Nutation spectroscopy of a nanomagnet driven into deeply nonlinear ferromagnetic resonance

Yi Li, Vladimir V. Naletov, Olivier Klein, José Luis Prieto, Manuel Muñoz, Vincent Cros, Paolo Bortolotti, Abdelmadjid Anane, Claudio Serpico, Grégoire de Loubens

▶ **To cite this version:**

Yi Li, Vladimir V. Naletov, Olivier Klein, José Luis Prieto, Manuel Muñoz, et al.. Nutation spectroscopy of a nanomagnet driven into deeply nonlinear ferromagnetic resonance. Physical Review X, 2019, 9, pp.041036. 10.1103/PhysRevX.9.041036 . hal-02063416

HAL Id: hal-02063416
https://hal.science/hal-02063416

Submitted on 12 Mar 2019

HAL is a multi-disciplinary open access archive for the deposit and dissemination of scientific research documents, whether they are published or not. The documents may come from teaching and research institutions in France or abroad, or from public or private research centers.

L'archive ouverte pluridisciplinaire **HAL**, est destinée au dépôt et à la diffusion de documents scientifiques de niveau recherche, publiés ou non, émanant des établissements d'enseignement et de recherche français ou étrangers, des laboratoires publics ou privés.

Nutation spectroscopy of a nanomagnet driven into deeply nonlinear ferromagnetic resonance

Y. Li,[1,*] V. V. Naletov,[1,2] O. Klein,[3] J. L. Prieto,[4] M. Muñoz,[5] V. Cros,[6] P. Bortolotti,[6] A. Anane,[6] C. Serpico,[7] and G. de Loubens[1,†]

[1]*Service de Physique de l'État Condensé, CEA, CNRS, Université Paris-Saclay, 91191 Gif-sur-Yvette, France*

[2]*Institute of Physics, Kazan Federal University, 420008 Kazan, Russian Federation*

[3]*Université Grenoble Alpes, CEA, CNRS, Grenoble INP, INAC-Spintec, 38000 Grenoble, France*

[4]*Instituto de Sistemas Optoelectrónicos y Microtecnología (UPM), 28040 Madrid, Spain*

[5]*Instituto de Microelectrónica de Madrid (CNM-CSIC), 28760 Madrid, Spain*

[6]*Unité Mixte de Physique CNRS, Thales, Univ. Paris-Sud, Université Paris-Saclay, 91767 Palaiseau, France*

[7]*Dipartimento di Ingegneria Elettrica e Tecnologie dell'Informazione, Università Federico II, 80138 Napoli, Italy*

(Dated: March 12, 2019)

Abstract

Strongly out-of-equilibrium regimes in magnetic nanostructures exhibit novel properties, linked to the nonlinear nature of magnetization dynamics, which are of great fundamental and practical interest. Here, we demonstrate that field-driven ferromagnetic resonance can occur with substantial spatial coherency at unprecedented large angle of magnetization precessions, which is normally prevented by the onset of spin-wave instabilities and magnetization turbulent dynamics. Our results show that this limitation can be overcome in nanomagnets, where the geometric confinement drastically reduces the density of spin-wave modes. The obtained deeply nonlinear ferromagnetic resonance regime is probed by a new spectroscopic technique based on the application of a second excitation field. This enables to resonantly drive slow coherent magnetization nutations around the large angle periodic trajectory. Our experimental findings are well accounted for by an analytical model derived for systems with uniaxial symmetry. They also provide new means for controlling highly nonlinear magnetization dynamics in nanostructures, which open interesting applicative opportunities in the context of magnetic nanotechnologies.

Spectroscopy based on the resonant interaction of electromagnetic fields with material media has been of tremendous impact on the development of physics since the beginning of the 20th century and remains of crucial importance till nowadays in the study of nanotechnologies. In this area, a central role is played by magnetic resonance spectroscopy, which includes various techniques such as nuclear magnetic resonance (NMR), electron paramagnetic resonance (EPR), and ferromagnetic resonance (FMR), all based on the excitation of the Larmor precession of magnetic moments around their equilibrium position [1].

FMR differs from NMR and EPR by the fact that in ferromagnetic media, magnetic moments are coupled by strong exchange interactions which tend to align them, leading to a large macroscopic spontaneous magnetization. In these conditions, magneto-dipolar effects become important and determine large internal fields which enrich both the ground state, that can be spatially non-uniform, and the dynamics of magnetic moments. The complex interactions taking place in the media can be described by an appropriate effective field which sets the time scale of the magnetization precession, and which itself depends on the magnetization, making the dynamics, for sufficiently large deviations from the ground state, highly nonlinear [2]. A special role in FMR is also played by the spin-waves (SWs), which are the collective eigenmodes associated to small magnetization oscillations around the equilibrium configuration [3]. When pumping fields excite SWs well above their thermal amplitudes, a rich variety of phenomena emerges, such as the formation of dynamical solitons [4, 5], SW turbulences and chaos [4, 6–8], and Bose-Einstein condensation of magnons [9], the quanta of SWs.

Recent developments in magnetic nanotechnologies have also demonstrated that FMR and SW dynamics can be excited either by microwave magnetic fields or by spin transfer torques, with the promise of innovative magnonic and spintronic devices for information and communication technologies [10]. In this area, spin torque nano-oscillators (STNOs) [11–15], which exhibit strong nonlinear properties [16], have even been successfully implemented to perform neuromorphic tasks [17, 18].

The complexity of magnetization dynamics when strongly nonlinear regimes set in is usually detrimental to the reliable control of nanomagnetic devices, such as oscillators, memories, and logic gates. In this respect, it is important to establish how far from equilibrium magnetic nanostructures can be driven before the coherent magnetization dynamics becomes highly perturbed by the onset of SW instabilities [19]. In this article, we provide a

crucial advancement in this problem. We demonstrate that FMR in a sufficiently confined nanostructure can exhibit unprecedented large angle magnetization precessions which are spatially quasi-uniform. The experimental evidence of the coherence of large precessions is brought by a new spectroscopic technique based on the application of a second probe excitation field, with frequency close to the one of the main time-harmonic field. This second excitation is used to drive small eigen oscillations of magnetization around the FMR large angle periodic oscillations, corresponding to coherent nutations of the magnetization. These nutation modes are substantially different from the usual SW modes around the ground state because they correspond to eigenmodes around a far-from-equilibrium state and their existence is connected to the one of a large coherent precession. Moreover, we show that the resonant excitation of these nutations can be used to control the nonlinear magnetization dynamics by affecting the switching fields associated with the bistability of the large angle FMR response pictured in Fig.1a, which occurs beyond the foldover instability predicted by Anderson and Suhl [20].

The preservation of coherent magnetization dynamics, which we report on a thin disc with sub-micrometric diameter, is mainly due to the geometric confinement. It significantly reduces the density of normal modes and suppresses the nonlinear SW interactions present in bulk ferromagnets [21, 22]. In addition, in our experiments the ground state is with the magnetization perpendicular to the plane. In this case, the uniform mode in thin films lies at the bottom of the SW manifold, so that it has no degenerate mode to couple to [23, 24] and the angle of the purely circular precession driven by FMR can reach large values [25]. These combined circumstances allow for the excitation of large-amplitude quasi-uniform precession of magnetization without simultaneous excitation of other SWs.

The experimental results of the present work also address the important issue of comparison between theory and experiments. In fact, by using the framework of dynamical systems [2], exact analytical solutions of the Landau-Lifshitz-Gilbert (LLG) equation in the presence of an arbitrarily large time-harmonic excitation have been found in high symmetry cases [26] and their stability analyzed [27], but have not been verified experimentally yet. For instance, the hysteretic FMR illustrated in Fig.1a has already been observed in measurements [28, 29], but with much weaker bistable response characteristics than expected from theory.

RESULTS

In the following, we investigate the FMR of an individual nanodisc of yttrium iron garnet (YIG) in the perpendicular configuration. The choice of YIG is natural as it is the magnetic material with the smallest SW damping, making it attractive to study weakly dissipative magnetization dynamics in the linear and nonlinear regimes [30]. The nanodisc has a diameter of 700 nm and is patterned from a 20 nm thick YIG film of magnetization $\mu_0 M_s = 0.21$ T [31], μ_0 being the vacuum permeability. It is saturated out-of-plane by a magnetic field $\boldsymbol{H}_0$ applied along its normal, z. A broadband antenna supplies a spatially uniform, linearly polarized microwave field of pulsation ω_1 oriented in the plane of the nanodisc. It can be decomposed into the left and right circularly polarized components, only the latter being efficiently coupled to the Larmor precession of the magnetization. In the following, h_1 will refer to the *circular* amplitude of the excitation field produced by the output power P_1 from the synthesizer. It drives the YIG nanodisc into FMR, thereby opening a precession angle θ of the magnetization $\boldsymbol{M}$ around $\boldsymbol{H}_0$ and decreasing its longitudinal component $M_z = M_s \cos\theta$. This dynamics is characterized by magnetic resonance force microscopy (MRFM), which sensitively probes the variation $\Delta M_z = M_s - M_z$ through the dipolar force between the YIG nanodisc and a magnetic nanosphere attached at the end of a soft cantilever [32], as sketched in Fig.1b. Further details about the sample, the MRFM set-up and the microwave calibration can be found in the Methods.

Linear spin-wave spectroscopy

In Fig.1c, the SW spectroscopy of the YIG nanodisc is performed at $\omega_1/(2\pi) = 10.5$ GHz and low power $P_1 = -30$ dBm, which is pulse modulated at the frequency of the MRFM cantilever to improve the signal to noise ratio. Quantized radial SW modes are excited by the uniform pumping field [33]. Their spatial profiles indexed by the radial number are shown above the spectrum. The fundamental Kittel mode is the one excited at the largest field, $\mu_0 H_K = 0.569$ T, and corresponds to a uniform phase of the transverse magnetization in the disc. Due to the geometric confinement, it is well separated from other SW modes at lower field [34]. Its full width at half maximum, $\mu_0 \Delta H = 0.35$ mT, is determined at even lower power ($P_1 = -38$ dBm) to avoid distortions of the resonance line due to the onset of foldover,

which occurs when the change in effective field becomes comparable to the FMR linewidth, at $P_1^{\rm th} = -33$ dBm or $\mu_0 h_1^{\rm th} = 0.009$ mT (see Methods). It corresponds to a Gilbert damping parameter $\alpha = \gamma\mu_0\Delta H/(2\omega_1) = 4.7 \cdot 10^{-4}$, where γ is the gyromagnetic ratio, in agreement with the value determined from broadband measurements (see Supplementary Fig.S1).

Deeply nonlinear FMR

The FMR spectrum of the YIG nanodisc radically changes at much stronger pumping fields. Fig.1d shows the measurement with a continuous wave (cw) excitation at $P_1 = +12$ dBm, *i.e.*, more than four orders of magnitude larger than the threshold of foldover instability. The cw excitation allows to reveal the bistable character of the nonlinear magnetization dynamics. By sweeping down the applied field (red curve) through the resonance of the Kittel mode, the precession angle substantially increases, which decreases the static demagnetizing field $\mu_0 M_z$ and shifts the FMR condition $\omega_1 = \gamma\mu_0(H_0 - M_z)$ to lower magnetic field by the same amount. This foldover shift to lower field continues until the pumping field cannot sustain anymore the large-amplitude magnetization dynamics, causing the sharp downward jump to the lower stable branch observed at $\mu_0 H_{\rm down} = 0.381$ T. By sweeping up the applied field (blue curve), an upward jump to the higher stable branch is observed at $\mu_0 H_{\rm up} = 0.516$ T. The extremely hysteretic foldover witnessed in this experiment is remarkable. Moreover, the maximal foldover shift $\mu_0(H_K - H_{\rm down}) = 0.188$ T corresponds to a reduction of nearly 90% of $\mu_0 M_z$ induced by the microwave pumping, which translates into a mean precession angle of 84° in the nanodisc. The evolution of the maximal normalized foldover shift as a function of the pumping field h_1 is plotted in Fig.1e together with $\Delta M_z^{\rm max}/M_s = 1 - \sqrt{1 - 4h_1^2/\Delta H^2}$ calculated from the macrospin LLG equation [3]. The measured foldover shift starts to deviate from the macrospin model beyond $\mu_0 h_1 \simeq 0.1$ mT, which is an order of magnitude larger than the threshold for foldover, when the angle of the uniform precession increases above 30°, corresponding to $\Delta M_z/M_s \simeq 15\%$. This is the signature of the onset of SW instabilities [19], which is here significantly postponed compared to what is observed in larger YIG samples, where the Suhl threshold is reached even before the onset of foldover, for a uniform precession angle of only a couple of degrees [35, 36]. In this respect, the experimental results presented in Fig.1 demonstrate that the discretization of the excitation spectrum in nanostructures efficiently inhibits nonlinear interactions between

SW modes, which drastically modifies the high amplitude magnetization dynamics [21, 22].

Nutation spectroscopy in the rotating frame

We now aim at probing the stability of the large-amplitude magnetization dynamics demonstrated above, which is periodic at ω_1 in the laboratory frame, hence referred to as **P**-mode [26]. In the frame rotating with $\boldsymbol{h}_1$ at ω_1 around the z-axis, the magnetization $\boldsymbol{M}_0$ of a **P**-mode is fixed at a polar angle θ_0 and a phase lag φ_0 (see Fig.2a and supplementary information). For this, we conduct two-tone measurements, where in addition to the strong cw excitation $\boldsymbol{h}_1$ at ω_1 a second weak microwave field $\boldsymbol{h}_2$, pulse modulated at the cantilever frequency, is applied at ω_2, as shown in Fig.2b. MRFM is used to simultaneously detect ΔM_1 induced by the main cw pumping at ω_1 (by monitoring the cantilever frequency, as in Fig.1d) and the additional change in longitudinal magnetization, ΔM_2, induced by the second excitation at ω_2 (by monitoring the amplitude of the cantilever vibrations, as in Fig.1c). The former informs us about the time-harmonic steady state regime driven by $\boldsymbol{h}_1$, whereas the latter allows us to spectroscopically probe the eigen excitations on top of this **P**-mode. The ΔM_2 spectrum measured at constant bias field $\mu_0 H_0 = 0.52$ T by sweeping $\omega_2/(2\pi)$ at low power $P_2 = -16$ dBm in the vicinity of the frequency $\omega_1/(2\pi) = 10.5$ GHz of the main pumping ($P_1 = +8$ dBm) is shown in Fig.2d. It displays two narrow resonance peaks centered at 10.2 GHz and 10.8 GHz, *i.e.*, symmetrically with respect to $\omega_1/(2\pi)$. This means that in the frame rotating with $\boldsymbol{h}_1$ at ω_1, the magnetization is precessing at $(\omega_2 - \omega_1)/(2\pi) = \pm\omega_{\mathrm{P},0}/(2\pi) = \pm 0.3$ GHz around its equilibrium position $\boldsymbol{M}_0$ (cf. Fig.2a). In other words, it is submitted to a slow nutation motion in the laboratory frame. The dependence of the nutation frequency $\omega_{\mathrm{P},0}$ on the main pumping field h_1 at fixed $\mu_0 H_0 = 0.52$ T is presented in Fig.2e, whereas its evolution measured as a function of the down swept field H_0 at fixed $P_1 = +8$ dBm and $P_1 = +1$ dBm is shown in the 2D spectroscopy maps of Fig.2f and 2h, respectively.

Following the theoretical approach of ref.[27], it is possible to calculate analytically the frequency $\omega_{\mathrm{P},0}$ of spatially uniform nutation around a given **P**-mode based on the macrospin LLG equation. Technical details are given in the Methods (the full derivation is presented in the supplementary information). In the limit of small damping, $\alpha \ll 1$, it can be expressed

as a function of h_1 and the angles θ_0 and φ_0 of the **P**-mode as follows:

$$\frac{\omega_{\mathrm{P},0}^2}{\gamma^2} = \frac{\mu_0 h_1 \cos\varphi_0}{\sin\theta_0}\left(\frac{\mu_0 h_1 \cos\varphi_0}{\sin\theta_0} + \mu_0 M_s \sin^2\theta_0\right). \quad (1)$$

This analytical expression is plotted as green dashed lines in Figs.2e, 2f and 2h, using the amplitude h_1 of the main driving field in the experiments, the angle of precession at the bias field H_0 determined from the normalized foldover shift, $\cos\theta_0 = (H_K - H_0)/M_s$, and the phase lag which satisfies $\gamma\mu_0 h_1 \sin\varphi_0 = \alpha\omega_1 \sin\theta_0$ in the macrospin model. It reproduces rather well the experimental data, except in regions where the level of excitation is very large, due to the deviation from the macrospin behavior already observed in Fig.1e. In addition, we have conducted full micromagnetic simulations in the time domain (see Methods), which allow us to extract the nutation frequency from the relaxation of the magnetization towards the steady state regime driven by $\boldsymbol{h}_1$, shown in Fig.2c. The obtained results, plotted as red dotted lines in Figs.2e, 2f and 2h, quantitatively agrees with the data on the full range of parameters investigated.

The dependence of the nutation frequency on h_1 observed in Fig.2e can be explained as follows. There is a minimum amplitude of $\mu_0 h_1 \simeq 0.15$ mT to drive the **P**-mode at $\mu_0 H_0 = 0.52$ T, which corresponds to a normalized foldover shift $(H_K - H_0)/M_s = 23\%$, *i.e.*, an angle of precession $\theta_0 \simeq 40°$. Above this amplitude, the nutation frequency is defined and increases with h_1 as predicted by Eq.1, which shows that there are two torques driving the nutation dynamics of the magnetization. The first one is linear, and directly provided by $\boldsymbol{h}_1$, which sets the Rabi frequency in a magnetic resonance experiment [37]. The second one is a demagnetizing torque specific to nonlinear FMR, which stiffens the nutation resonance.

We now interpret the nutation spectroscopy maps of Figs.2f and 2h, where ΔM_2 is measured at fixed h_1 by sweeping H_0 and ω_2. When $H_0 > H_K$, the magnetization dynamics is driven off resonantly by $\boldsymbol{h}_1$ and has small amplitude. Hence, the weak microwave field $\boldsymbol{h}_2$ simply excites the linear Kittel resonance on top of it, which explains the bright linear dispersion $\omega_2 = \gamma\mu_0(H_0 - M_s)$ observed in this region. The situation is quite different when $H_0 < H_K$. In this case, $\boldsymbol{h}_1$ drives the strong foldover regime demonstrated in Fig.1 upon sweeping down H_0, and $\boldsymbol{h}_2$ excites the magnetization dynamics on top of the corresponding **P**-mode. The evolution of the two resonance branches symmetrically distributed around the main pumping frequency ω_1 as a function of H_0 is reproduced qualitatively by Eq.1, and quantitatively by micromagnetic simulations. The fact that the upper branch is continuous

with the linear Kittel resonance branch observed above H_K indicates that the perturbation of the **P**-mode driven by $\boldsymbol{h}_2$ has a uniform phase, *i.e.*, corresponds to a uniform nutation of the magnetization.

The experimental results presented in Fig.2 also demonstrate that the weak resonant excitation of the nutation mode can destabilize the strong foldover dynamics. Figs.2g and 2i display the evolution of ΔM_1 induced by the cw pumping $\boldsymbol{h}_1$ at ω_1, while exciting the nutation dynamics with $\boldsymbol{h}_2$ as a function of H_0 and ω_2, whose ΔM_2 spectroscopy is presented in Figs.2f and 2h, respectively. In these 2D maps, the foldover breakdown occurring at H_{down} is easily identified thanks to the associated sharp change of ΔM_1, and is anticipated as the nutation mode is excited. This is particularly clear in Fig.2i, where the maximal foldover shift $\mu_0(H_K - H_{\text{down}})$ is reduced by almost 0.05 T when $|\omega_2 - \omega_1|/(2\pi) \simeq 0.2$ GHz, which corresponds to the nutation resonance. Moreover, these data suggest that higher order nutation modes can be excited by $\boldsymbol{h}_2$, since an anticipated foldover breakdown is also observed at $|\omega_2 - \omega_1|/(2\pi) \simeq 0.35$ GHz.

In order to investigate these other nutation modes, we perform the same measurements as in Figs.2f–i, but for larger detunings $\omega_2 - \omega_1$ (P_2 is also increased from -19 to -13 dBm). The results obtained at $P_1 = +1$ dBm are reported in Figs.3b–c (those obtained at $P_1 = +8$ dBm are presented in Supplementary Fig.S2). The spectroscopy map of the SW modes excited by $\boldsymbol{h}_2$ in the absence of $\boldsymbol{h}_1$ is shown in Fig.3a. It displays the linear dispersion relation of the radial SW modes excited by the uniform field $\boldsymbol{h}_2$, already discussed in Fig.1c. Due to the strong foldover regime driven by $\boldsymbol{h}_1$ at $H_0 < H_K$ in Fig.3b, each of these radial SW branches transforms into a pair of branches symmetric around ω_1. Additionally, there is a pair of branches which appears at twice the main nutation frequency, which is due to the ellipticity of the trajectory, apparent on Fig.2c. The macrospin approach used to derive Eq.1 cannot be used to account for these higher order nutation modes, although plane wave perturbations to the **P**-mode can also be analytically calculated [27]. We therefore use micromagnetic simulations to calculate the SW nutation spectra shown in Fig.3d, which are in good agreement with the experiments. The extracted SW nutation modes profiles (see Methods), shown as insets in Fig.3d, indicate that there is some continuity between the radial SW modes excited in the linear regime on top of the equilibrium magnetization and the nutation modes excited on top of the **P**-mode driven in the nonlinear regime by $\boldsymbol{h}_1$. Finally, Fig.3c confirms that the excitation of the nutation resonances can destabilize the

strong foldover dynamics.

DISCUSSION

As in the case of a spinning top, the nutation of magnetization demonstrated above is made possible by the specific properties of the dynamics on the unit sphere [2]. Namely, it is topologically allowed for the magnetization to oscillate around its fixed point $\boldsymbol{M}_0\ (\theta_0, \varphi_0)$ in the rotating frame, which is set by the drive $\boldsymbol{h}_1$. The nutation frequency results from the balance of torques acting on the angular momentum, and is given by Eq.1 in the case of a macrospin governed by the LLG equation. The accuracy of the latter to account for the experimental data means that the coherent precession of the magnetization vector is dominating the deeply nonlinear driven dynamics, despite the signatures of SW instabilities observed at very large pumping power. Their main effect is to slightly reduce the nutation frequency, which is well captured by full micromagnetic simulations. This can be ascribed to the shift of the phase between the pumping field and the average magnetization [38] observed in our simulations, a key effect to explain the above threshold dynamics [7, 39]. The nutation spectroscopy of magnetization thus allows a more detailed investigation of the highly nonlinear regime, where auto-oscillation instabilities [6, 23, 40, 41] and instability patterns [42] have been evidenced. Moreover, its quantitative understanding, made possible thanks to the low density of SW modes in nanomagnets, should enable to test further the LLG equation governing the motion of magnetization against experimental measurements.

Our results also highlight that the dynamical states driven by a high power microwave signal can be controlled using a second signal with much lower power by the resonant excitation of the nutation modes. This could be applied in devices taking advantages of the bistable magnetization dynamics for microwave signal processing [28], in analogy to microwave assisted magnetization switching [43–45]. Furthermore, the frequency selectivity and energy efficiency of nutation excitations provide new potentials for the scheme of neuromorphic computing. Cognitive tasks have already been implemented using the nonlinear dynamics of nanomagnets, from the transient regime of a single STNO [17] to the collective behavior of mutually coupled STNOs controlled by external microwave signals [18, 46]. An appropriate use of the nutation dynamics of magnetization would allow to gain additional control on nonlinear dynamics, which is highly desired in this field.

METHODS

Sample preparation. A 20 nm thick $Y_3Fe_5O_{12}$ (YIG) film was grown by pulsed laser deposition on a (111) $Gd_3Ga_5O_{12}$ (GGG) substrate, as described in ref.[31]. It was used to pattern the studied YIG nanodisc by electron lithography and dry etching. After the insertion of a 50 nm thick SiO_2 insulating layer, a 150 nm thick and 5 μm wide gold antenna was defined on top of the nanodisc to provide the microwave excitation [34].

MRFM set-up. The magnetic resonance force microscope is located between the poles of an electromagnet and operated under vacuum (10^{-6} mbar) at a stabilized temperature of 288 K. The cantilever is an Olympus Biolever (spring constant 5 mN·m^{-1}) with a 700-nm-diameter sphere of an amorphous FeSi alloy (magnetic moment 0.28 pA·m^2) glued to its apex. In this study, MRFM spectroscopy is achieved by placing the center of this magnetic nanosphere at a distance of 1.5–1.8 μm above the center of the YIG nanodisc. The strayfield of the MRFM probe (10–16 mT) is subtracted from the corresponding spectra. The displacement of the cantilever is monitored using optical techniques. Its mechanical frequency ($f_c \approx 12.3$ kHz) is tracked using a phase-locked loop and its vibration amplitude stabilized to 4 nm using a piezoelectric bimorph. When the cw microwave pumping excites the magnetization dynamics in the sample, its longitudinal component is reduced, so the static dipolar force with the magnetic probe diminishes. The associated variation of the cantilever frequency provides a quantitative magnetometry of the sample [47]. In order to improve the signal to noise ratio, the microwave excitation is pulsed on and off at f_c. In that case, the cantilever vibrations induced by the magnetization dynamics excited in the sample are enhanced by the quality factor $Q \approx 2000$ of the mechanical detection [32].

Microwave field calibration. We use the onset of foldover as a mean to calibrate the amplitude of the excitation field produced by the microwave antenna at the sample location [33]. At the threshold of foldover instability $h_1^{\rm th} = 0.62\Delta H^{3/2}/M_s^{1/2}$ [20], and the slope of the FMR curve becomes infinite on the low field side of the resonance, which is experimentally observed at 10.5 GHz for an output power from the synthesizer $P_1^{\rm th} = -33$ dBm. Using the FMR line width measured in the linear regime, one gets $\mu_0 h_1^{\rm th} = 0.009$ mT, *i.e.*, a calibration factor $a = 0.4$ mT$/\sqrt{\rm mW}$ between microwave field and power. To get a better precision, we also fit the dependences on power of the critical fields $H_{\rm down}$ and $H_{\rm up}$ determined experimentally beyond the foldover onset [29], which yields $a = 0.41 \pm 0.03$ mT$/\sqrt{\rm mW}$.

Analytical calculations. The nonlinear FMR excited in a uniaxial system by the superposition of two time-harmonic external fields, $\boldsymbol{h}_{\rm ac}(t) = \boldsymbol{h}_1(t) + \boldsymbol{h}_2(t)$ with $|\boldsymbol{h}_2(t)| \ll |\boldsymbol{h}_1(t)|$, is calculated based on the macrospin LLG equation. The main stages of the analytical derivation presented in the supplementary information are the following. The LLG equation is first written in the frame of reference rotating around the z-axis at the angular frequency ω_1 of the dominant time-harmonic component: $\dot{\boldsymbol{m}} - \alpha \boldsymbol{m} \times \dot{\boldsymbol{m}} = -\boldsymbol{m} \times (\boldsymbol{h}_{\rm eff} - \omega_1 \boldsymbol{e}_z) + \alpha\omega_1 \boldsymbol{m} \times (\boldsymbol{e}_z \times \boldsymbol{m})$ where $\boldsymbol{h}_{\rm eff} = \kappa_{\rm eff} m_z \boldsymbol{e}_z + h_0 \boldsymbol{e}_z + \boldsymbol{h}_{\rm ac}(t)$, $\dot{\boldsymbol{m}}$ is the time derivative of the normalized magnetization vector taken in the rotating frame, $\boldsymbol{h}_0$ the normalized bias field, $\boldsymbol{e}_z$ the unit vector along it, and $\kappa_{\rm eff}$ the effective anisotropy constant. It is then written in spherical coordinates and considered in the case where only the right circularly polarized component of $\boldsymbol{h}_1$ is applied. This allows to find its equilibrium points $\boldsymbol{m}_0$ (**P**-modes), or equivalently (θ_0, φ_0), and to analyze the foldover of FMR [26]. The standard analysis of the stability of these **P**-modes allows to calculate the nutation frequency given in Eq.1 [27]. Shortly, $\boldsymbol{m}$ is expanded around $\boldsymbol{m}_0$ to linearize the LLG equation, and the complex amplitudes of magnetization perturbations are calculated in the rotating frame by projecting them in the plane $(\boldsymbol{e}_1, \boldsymbol{e}_2)$ orthogonal to $\boldsymbol{m}_0$, where $\sin\theta_0 \boldsymbol{e}_1 = (\boldsymbol{e}_z \times \boldsymbol{m}_0) \times \boldsymbol{m}_0$ and $\sin\theta_0 \boldsymbol{e}_2 = (\boldsymbol{e}_z \times \boldsymbol{m}_0)$. Finally, the **P**-mode linear response to the small additional microwave field $\boldsymbol{h}_2$ is studied.

Micromagnetic simulations. The magnetization dynamics in the YIG nanodisc is calculated using the python module MicroMagnum, a micromagnetic finite difference simulator which can be runned on GPU [48]. The nominal geometry of the nanodisc (diameter 700 nm, thickness 20 nm) is discretized using a $128 \times 128 \times 1$ rectangular mesh. The following magnetic parameters are used: $M_s = 1.67 \cdot 10^5$ A·m^{-1}, $A_{\rm ex} = 4.3 \cdot 10^{-12}$ J·m^{-1} (exchange length $\simeq 16$ nm), $\gamma/(2\pi) = 28.5$ GHz·T^{-1}·s^{-1}, and $\alpha = 5 \cdot 10^{-4}$. The bias magnetic field is applied along the normal of the disc. The static equilibrium configuration of the magnetization is calculated at 0.59 T. Then a linearly polarized excitation field of constant amplitude is applied at 10.5 GHz in the plane of the disc, and for each value of the bias magnetic field, which is decreased by steps of 0.02 T, the resulting magnetization dynamics is calculated over 100 ns with a typical step of 3 ps. This allows to reproduce the foldover regime demonstrated in the experiments and to calculate the nutation frequencies. Those are obtained by fast Fourier transformation of the transient dynamics of the average magnetization simulated at each bias field. The nutation mode profiles are obtained by stroboscopically averaging the magnetization dynamics at the corresponding nutation frequencies in the rotating frame.

ACKNOWLEDGEMENTS

Y.L. thanks the French National Research Agency for funding under contract No. ANR-14-CE26-0021 (MEMOS), V.V.N. the Russian Competitive Growth program of KFU, and C.S. the Labex NanoSaclay for support under the action "Rayonnement International". This research was partially funded by the ANR-18-CE24-0021 (MAESTRO) project.

---

* Currently at Materials Science Division, Argonne National Laboratory, Argonne (IL), USA

† gregoire.deloubens@cea.fr

[1] C. Kittel, *Introduction to Solid State Physics*, 8th ed. (Wiley, 2004).

[2] I. D. Mayergoyz, G. Bertotti, and C. Serpico, *Nonlinear magnetization dynamics in nanosystems* (Elsevier, 2009).

[3] A. G. Gurevich and G. A. Melkov, *Magnetization Oscillations and Waves* (CRC Press, 1996).

[4] P. E. Wigen, ed., *Nonlinear Phenomena and Chaos in Magnetic Materials* (World Scientific-World Scientific, Singapore, 1994).

[5] S. M. Mohseni, S. R. Sani, J. Persson, T. N. Anh Nguyen, S. Chung, Ye. Pogoryelov, P. K. Muduli, E. Iacocca, A. Eklund, R. K. Dumas, S. Bonetti, A. Deac, M. A. Hoefer, and J. Akerman, "Spin torque-generated magnetic droplet solitons," Science **339**, 1295–1298 (2013).

[6] S. M. Rezende and F. M. de Aguiar, "Spin-wave instabilities, auto-oscillations, and chaos in yttrium-iron-garnet," Proc. IEEE **78**, 893–908 (1990).

[7] Victor S. L'vov, *Wave Turbulence Under Parametric Excitation: Applications to Magnets* (Springer-Verlag, 1994).

[8] S. Petit-Watelot, J.-V. Kim, A. Ruotolo, R. M. Otxoa, K. Bouzehouane, J. Grollier, A. Vansteenkiste, B. Van de Wiele, V. Cros, and T. Devolder, "Commensurability and chaos in magnetic vortex oscillations," Nature Phys. **8**, 682–687 (2012).

[9] S. O. Demokritov, V. E. Demidov, O. Dzyapko, G. A. Melkov, A. A. Serga, B. Hillebrands, and A. N. Slavin, "Bose–Einstein condensation of quasi-equilibrium magnons at room temperature under pumping," Nature **443**, 430–433 (2006).

[10] A. V. Chumak, V. I. Vasyuchka, A. A. Serga, and B. Hillebrands, "Magnon spintronics," Nature Phys. **11**, 453–461 (2015).

[11] S. I. Kiselev, J. C. Sankey, I. N. Krivorotov, N. C. Emley, R. J. Schoelkopf, R. A. Buhrman, and D. C. Ralph, "Microwave oscillations of a nanomagnet driven by a spin-polarized current," Nature **425**, 380–383 (2003).

[12] D. Houssameddine, U. Ebels, B. Delat, B. Rodmacq, I. Firastrau, F. Ponthenier, M. Brunet, C. Thirion, J.-P. Michel, L. Prejbeanu-Buda, M.-C. Cyrille, O. Redon, and B. Dieny, "Spin-torque oscillator using a perpendicular polarizer and a planar free layer," Nature Mater. **6**, 447–453 (2007).

[13] W. Chen, G. de Loubens, J.-M. L. Beaujour, J. Z. Sun, and A. D. Kent, "Spin-torque driven ferromagnetic resonance in a nonlinear regime," Appl. Phys. Lett. **95**, 172513 (2009).

[14] A. Hamadeh, G. de Loubens, V. V. Naletov, J. Grollier, C. Ulysse, V. Cros, and O. Klein, "Autonomous and forced dynamics in a spin-transfer nano-oscillator: Quantitative magnetic-resonance force microscopy," Phys. Rev. B **85**, 140408 (2012).

[15] M. Collet, X. de Milly, O. d'Allivy Kelly, V.V. Naletov, R. Bernard, P. Bortolotti, J. Ben Youssef, V.E. Demidov, S.O. Demokritov, J.L. Prieto, M. Muñoz, V. Cros, A. Anane, G. de Loubens, and O. Klein, "Generation of coherent spin-wave modes in yttrium iron garnet microdiscs by spin-orbit torque," Nature Commun. **7**, 10377 (2016).

[16] A. Slavin and V. Tiberkevich, "Nonlinear auto-oscillator theory of microwave generation by spin-polarized current," IEEE Trans. Magn. **45**, 1875–1918 (2009).

[17] J. Torrejon, M. Riou, F. Abreu Araujo, S. Tsunegi, G. Khalsa, D. Querlioz, P. Bortolotti, V. Cros, K. Yakushiji, A. Fukushima, H. Kubota, S. Yuasa, M. D. Stiles, and J. Grollier, "Neuromorphic computing with nanoscale spintronic oscillators," Nature **547**, 428–431 (2017).

[18] M. Romera, P. Talatchian, S. Tsunegi, F. Abreu Araujo, V. Cros, P. Bortolotti, J. Trastoy, K. Yakushiji, A. Fukushima, H. Kubota, *et al.*, "Vowel recognition with four coupled spin-torque nano-oscillators," Nature **563**, 230–234 (2018).

[19] H. Suhl, "The theory of ferromagnetic resonance at high signal powers," J. Phys. Chem. Solids **1**, 209–227 (1957).

[20] P. W. Anderson and H. Suhl, "Instability in the motion of ferromagnets at high microwave power levels," Phys. Rev. **100**, 1788–1789 (1955).

[21] Y. Kobljanskyj, G. Melkov, K. Guslienko, V. Novosad, S. D. Bader, M. Kostylev, and A. Slavin, "Nano-structured magnetic metamaterial with enhanced nonlinear properties," Sci. Rep. **2**, 478 (2012).

[22] G.A. Melkov, D.V. Slobodianiuk, V.S. Tiberkevich, G. de Loubens, O. Klein, and A.N. Slavin, "Nonlinear ferromagnetic resonance in nanostructures having discrete spectrum of spin-wave modes," IEEE Magn. Lett. **4**, 4000504 (2013).

[23] R. D. McMichael and P. E. Wigen, "High-power ferromagnetic resonance without a degenerate spin-wave manifold," Phys. Rev. Lett. **64**, 64–67 (1990).

[24] Yu. V. Gulyaev, P. E. Zil'berman, A. G. Temiryazev, and M. P. Tikhomirova, "Principal mode of the nonlinear spin-wave resonance in perpendicular magnetized ferrite films," Phys. Solid State **42**, 1094–1099 (2000).

[25] K. Gnatzig, H. Dötsch, M. Ye, and A. Brockmeyer, "Ferrimagnetic resonance in garnet films at large precession angles," J. Appl. Phys. **62**, 4839–4843 (1987).

[26] G. Bertotti, C. Serpico, and I. D. Mayergoyz, "Nonlinear magnetization dynamics under circularly polarized field," Phys. Rev. Lett. **86**, 724–727 (2001).

[27] G. Bertotti, I. D. Mayergoyz, and C. Serpico, "Spin-wave instabilities in large-scale nonlinear magnetization dynamics," Phys. Rev. Lett. **87**, 217203 (2001).

[28] Y.K. Fetisov, Carl E. Patton, and V.T. Synogach, "Nonlinear ferromagnetic resonance and foldover in yttrium iron garnet thin films – inadequacy of the classical model," IEEE Trans. Magn. **35**, 4511–4521 (1999).

[29] Y. S. Gui, A. Wirthmann, and C.-M. Hu, "Foldover ferromagnetic resonance and damping in permalloy microstrips," Phys. Rev. B **80**, 184422 (2009).

[30] A. A. Serga, A. V. Chumak, and B. Hillebrands, "YIG magnonics," J. Phys. D: Appl. Phys. **43**, 264002 (2010).

[31] O. d'Allivy Kelly, A. Anane, R. Bernard, J. Ben Youssef, C. Hahn, A H. Molpeceres, C. Carretero, E. Jacquet, C. Deranlot, P. Bortolotti, R. Lebourgeois, J.-C. Mage, G. de Loubens, O. Klein, V. Cros, and A. Fert, "Inverse spin hall effect in nanometer-thick yttrium iron garnet/Pt system," Appl. Phys. Lett. **103**, 082408 (2013).

[32] O. Klein, G. de Loubens, V. V. Naletov, F. Boust, T. Guillet, H. Hurdequint, A. Leksikov, A. N. Slavin, V. S. Tiberkevich, and N. Vukadinovic, "Ferromagnetic resonance force spectroscopy of individual submicron-size samples," Phys. Rev. B **78**, 144410 (2008).

[33] V. V. Naletov, G. de Loubens, G. Albuquerque, S. Borlenghi, V. Cros, G. Faini, J. Grollier, H. Hurdequint, N. Locatelli, B. Pigeau, A. N. Slavin, V. S. Tiberkevich, C. Ulysse, T. Valet, and O. Klein, "Identification and selection rules of the spin-wave eigenmodes in a normally

magnetized nanopillar," Phys. Rev. B **84**, 224423 (2011).

[34] C. Hahn, V. V. Naletov, G. de Loubens, O. Klein, O. d'Allivy Kelly, A. Anane, R. Bernard, E. Jacquet, P. Bortolotti, V. Cros, J. L. Prieto, and M. Muñoz, "Measurement of the intrinsic damping constant in individual nanodisks of $Y_3Fe_5O_{12}$ and $Y_3Fe_5O_{12}$|Pt," Appl. Phys. Lett. **104**, 152410 (2014).

[35] G. de Loubens, V. V. Naletov, and O. Klein, "Reduction of the spin-wave damping induced by nonlinear effects," Phys. Rev. B **71**, 180411 (2005).

[36] V. V. Naletov, V. Charbois, O. Klein, and C. Fermon, "Quantitative measurement of the ferromagnetic resonance signal by force detection," Appl. Phys. Lett. **83**, 3132 (2003).

[37] Amir Capua, Charles Rettner, See-Hun Yang, Timothy Phung, and Stuart S. P. Parkin, "Ensemble-averaged rabi oscillations in a ferromagnetic CoFeB film," Nature Commun. **8**, 16004 (2017).

[38] Hans G. Bauer, Peter Majchrak, Torsten Kachel, Christian H. Back, and Georg Woltersdorf, "Nonlinear spin-wave excitations at low magnetic bias fields," Nature Commun. **6**, 8274 (2015).

[39] T. Gerrits, P. Krivosik, M. L. Schneider, C. E. Patton, and T. J. Silva, "Direct Detection of Nonlinear Ferromagnetic Resonance in Thin Films by the Magneto-Optical Kerr Effect," Phys. Rev. Lett. **98**, 207602 (2007).

[40] B. Lührmann, M. Ye, H. Dötsch, and A. Gerspach, "Nonlinearities in the ferrimagnetic resonance in epitaxial garnet films," J. Magn. Magn. Mater. **96**, 237–244 (1991).

[41] S. Watanabe, D. Hirobe, Y. Shiomi, R. Iguchi, S. Daimon, M. Kameda, S. Takahashi, and E. Saitoh, "Generation of megahertz-band spin currents using nonlinear spin pumping." Sci. Rep. **7**, 4576 (2017).

[42] R. Bonin, M. d'Aquino, G. Bertotti, C. Serpico, and I. D. Mayergoyz, "Analysis of magnetization instability patterns in spin-transfer nano-oscillators," Eur. Phys. J. B **85**, 47 (2012).

[43] C. Thirion, W. Wernsdorfer, and D. Mailly, "Switching of magnetization by nonlinear resonance studied in single nanoparticles," Nature Mater. **2**, 524–527 (2003).

[44] B. Pigeau, G. de Loubens, O. Klein, A. Riegler, F. Lochner, G. Schmidt, and L. W. Molenkamp, "Optimal control of vortex-core polarity by resonant microwave pulses," Nature Phys. **7**, 26–31 (2011).

[45] Hirofumi Suto, Taro Kanao, Tazumi Nagasawa, Koichi Mizushima, and Rie Sato, "Magnetization switching of a Co/Pt multilayered perpendicular nanomagnet assisted by a microwave

field with time-varying frequency," Phys. Rev. Appl. **9**, 054011 (2018).

[46] Yi Li, Xavier de Milly, Flavio Abreu Araujo, Olivier Klein, Vincent Cros, Julie Grollier, and Grégoire de Loubens, "Probing phase coupling between two spin-torque nano-oscillators with an external source," Phys. Rev. Lett. **118**, 247202 (2017).

[47] H. Lavenant, V. Naletov, O. Klein, G. de Loubens, L. Casado, and J. M. De Teresa, "Mechanical magnetometry of cobalt nanospheres deposited by focused electron beam at the tip of ultra-soft cantilevers," Nanofabrication **1**, 65–73 (2014).

[48] http://micromagnum.informatik.uni-hamburg.de/.

FIGURES

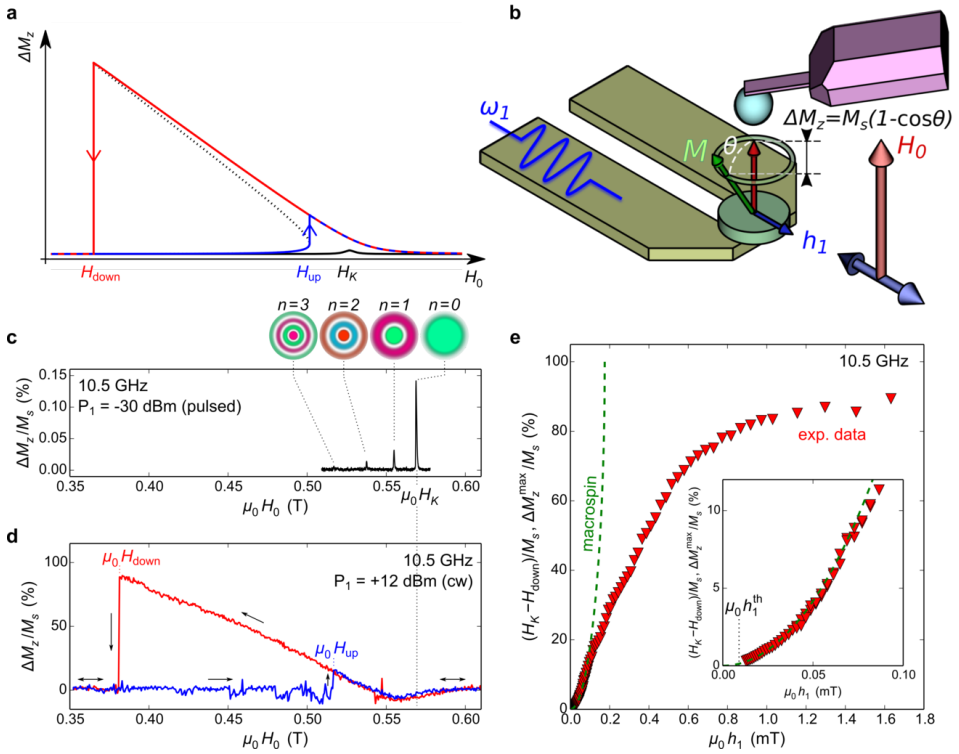


FIG. 1. **Ultrastrong foldover of FMR.** (a) Illustration of hysteretic foldover in the nonlinear regime of FMR, where jumps between the two stable branches of the dynamics occur at $H_{\rm down}$ and $H_{\rm up}$. The dotted line is the unstable branch. The black Lorentzian curve centered at H_K corresponds to linear FMR. (b) Schematics of the experiment. A microwave field $\boldsymbol{h}_1$ of pulsation ω_1 drives the magnetization $\boldsymbol{M}$ of a YIG nanodisc into FMR, opening a precession angle θ around the perpendicularly applied field $\boldsymbol{H}_0$. The associated variation in the longitudinal component of the magnetization, ΔM_z, is mechanically detected by the cantilever of a magnetic resonance force microscope. (c) Spin-wave spectroscopy performed at 10.5 GHz in the linear regime. The profiles of the quantized radial SW modes, calculated using a micromagnetic code, are shown above (different colors display regions precessing in opposite phase). (d) FMR spectrum in the deeply nonlinear regime exhibiting ultrastrong hysteretic foldover and nearly complete suppression of M_z. (e) Evolution of the maximal normalized foldover shift as a function of the pumping field h_1. The dashed line shows the behavior expected for a macrospin and the inset a zoomed view of the low amplitude regime.

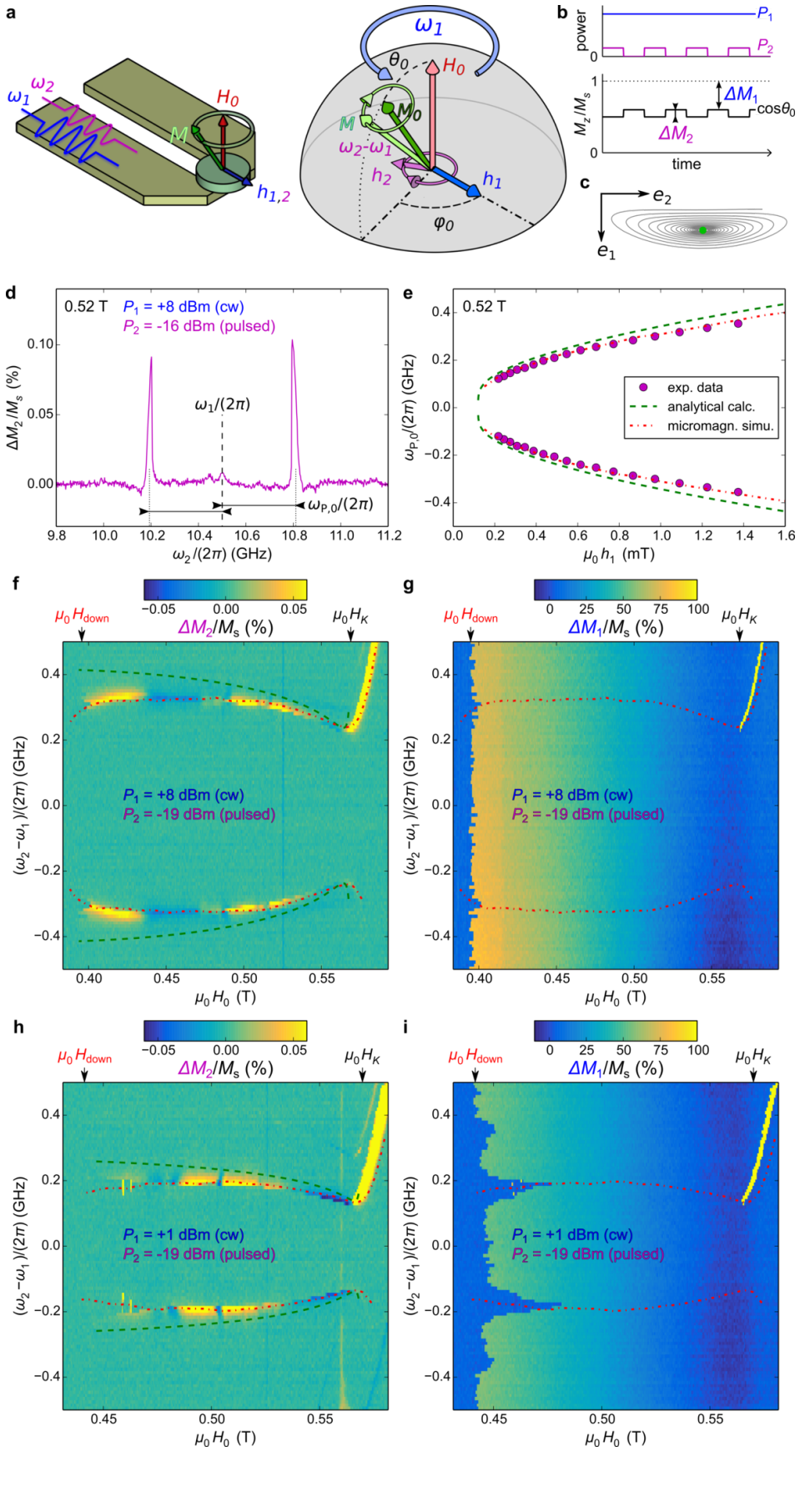

a
b
c
d
e
f
g
h
i
power
time
exp. data
analytical calc.
micromagn. simu.
0.52 T
P1 = +8 dBm (cw)
P2 = -16 dBm (pulsed)
P1 = +8 dBm (cw)
P2 = -19 dBm (pulsed)
P1 = +1 dBm (cw)
P2 = -19 dBm (pulsed)
ΔM2/Ms (%)
ΔM1/Ms (%)
μ0 Hdown
μ0 HK
μ0 H0 (T)
μ0 h1 (mT)
ω2/(2π) (GHz)
(ω2−ω1)/(2π) (GHz)
ωP,0/(2π) (GHz)

FIG. 2. **Nutation of magnetization.** (a,b) Principle of the experiment. A low power pulse modulated microwave field $\boldsymbol{h}_2$ of pulsation ω_2 is added to the main pumping cw field $\boldsymbol{h}_1$. This enables the spectroscopy in the frame rotating with $\boldsymbol{h}_1$ at ω_1, where the magnetization $\boldsymbol{M}_0$ of the **P**-mode is fixed at an angle θ_0 and a phase lag φ_0. (c) Relaxation trajectory of the magnetization towards the **P**-mode in the plane $(\boldsymbol{e}_1, \boldsymbol{e}_2)$ orthogonal to $\boldsymbol{M}_0$ defined in the Methods, calculated using micromagnetic simulations. (d) Spectroscopy performed at $\omega_1/(2\pi) = 10.5$ GHz and $\mu_0 H_0 = 0.52$ T as a function of ω_2. The two resonance peaks symmetric with respect to ω_1 correspond to a motion of nutation in the laboratory frame. (e) Evolution of the nutation frequency as a function of the main pumping field h_1 at fixed $\mu_0 H_0 = 0.52$ T. (f) Nutation spectroscopy map at fixed h_1 of the small amplitude dynamics ΔM_2 excited by ω_2 as a function of the down swept field H_0. (g) Simultaneous measurement of ΔM_1 induced by the main pumping at ω_1. (h,i) Same as (f,g) for a smaller main pumping power. In panels (e)–(i), the green dashed lines show the analytical predictions from Eq.1 and red dotted lines the results from micromagnetic simulations.

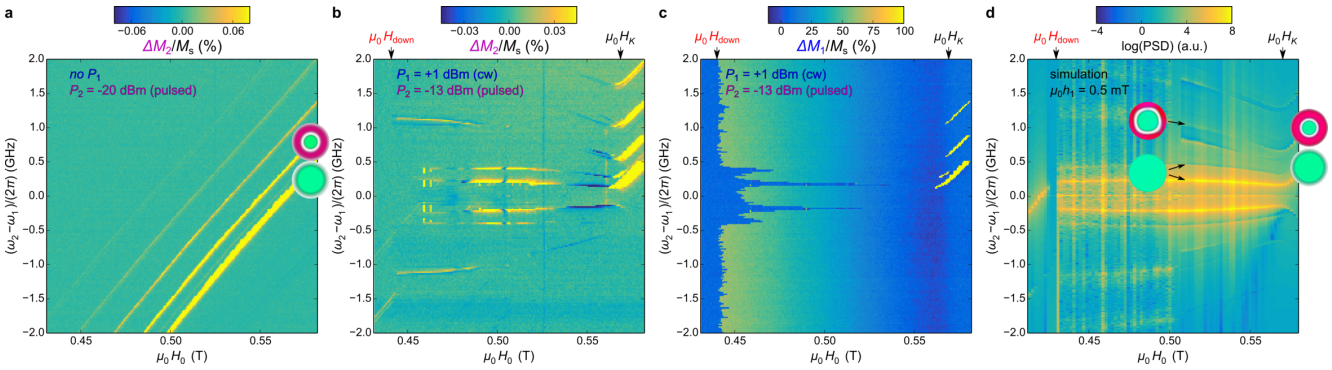


FIG. 3. **Spin-wave nutation modes.** (a) Spectroscopy map of the SW modes excited by the low power excitation at ω_2 *in the absence* of the main pumping at $\omega_1/(2\pi) = 10.5$ GHz. They correspond to the same radial modes as probed in the linear regime in Fig.1c, whose profiles are recalled as insets. (b) ΔM_2 spectroscopy map of the SW nutation modes excited by the low power excitation at ω_2 *in the presence* of the main excitation at ω_1 ($P_1 = +1$ dBm). (c) Simultaneous measurement of ΔM_1 induced by the main pumping at ω_1. (d) Micromagnetic simulations of the experimental data shown in (b). The SW mode profiles shown as insets are extracted at some specific $\omega_2 - \omega_1$ and H_0. In all the panels, the perpendicular field H_0 is swept down.

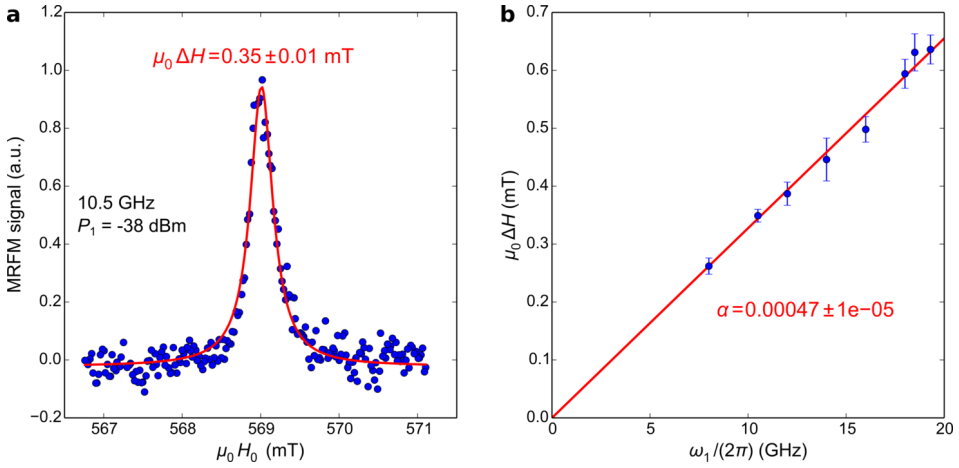


FIG. 4. (Supplementary Fig.S1) **Gilbert damping of the YIG nanodisc.** (a) FMR peak measured at $\omega_1/(2\pi) = 10.5$ GHz and $P_1 = -38$ dBm. A Lorentzian fit to the data yields the full width at half maximum $\mu_0\Delta H$ together with the associated error bar. (b) Dependence on excitation frequency of $\mu_0\Delta H$ determined in the linear regime. A linear fit to the data yields the Gilbert damping parameter of the YIG nanodisc.

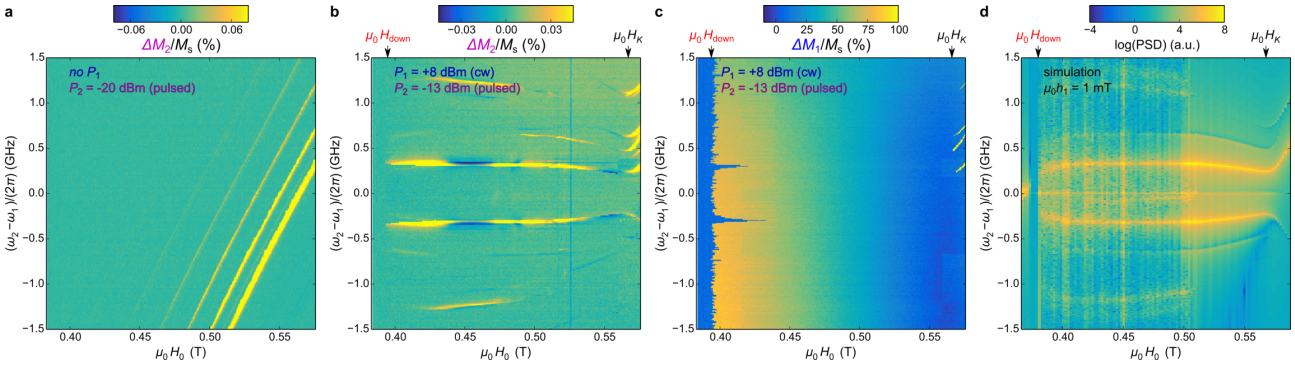


FIG. 5. (Supplementary Fig.S2) **Spin-wave nutation modes at larger main pumping power.** (a) Spectroscopy map of the SW modes excited by the low power excitation at ω_2 *in the absence* of the main pumping at $\omega_1/(2\pi) = 10.5$ GHz. (b) ΔM_2 spectroscopy map of the SW nutation modes excited by the low power excitation at ω_2 *in the presence* of the main excitation at ω_1 ($P_1 = +8$ dBm). (c) Simultaneous measurement of ΔM_1 induced by the main pumping at ω_1. (d) Micromagnetic simulations of the experimental data shown in (b). In all the panels, the perpendicular field H_0 is swept down.